Transient analysis of the transmitting properties of a focused acoustic transducer with an arbitrary rim

Adrianus T. de Hoop,[a] Smaine Zeroug, and Sergio Kostek
Schlumberger-Doll Research, Old Quarry Road, Ridgefield, Connecticut 06877-4108

(Received 26 December 1994; revised 20 March 1995; accepted 3 April 1995)

Closed-form analytic expressions are derived for the efficient calculation of the transient acoustic wave field emitted by a focused transducer with a spherical surface. The radiated transient acoustic wave field is evaluated by applying the Maggi–Rubinowicz transformation to the Kirchhoff–Huygens representation of the wave field. This transformation results in a line integral representation along the rim of the radiating aperture that holds for a rim of arbitrary shape, and for both planar and nonplanar radiators. The line integral is readily evaluated numerically and the results are used to study the shape of the beam emitted by the transducer in its dependence on the shape of the rim. This is shown through numerical results for a spherical-cap transducer and a spherically curved rectangular-strip transducer. The computation time needed to evaluate the (one-dimensional) integrals is in the order of seconds on a standard workstation. © *1995 Acoustical Society of America.*

PACS numbers: 43.20.Px, 43.30.Vh, 43.38.Ar

INTRODUCTION

The standard method for analyzing the transient behavior of acoustic transducers is to start from the Kirchhoff–Huygens representation for the acoustic pressure of the emitted wave field. In this representation, the values of the acoustic pressure and of the normal component of the particle velocity at the radiating aperture of the transducer occur. For these quantities, an *Ansatz* is made and the relevant surface integral is evaluated. This technique has been worked out for planar and spherically curved transducers, starting from the Rayleigh formulas, which are the appropriate starting points for calculating the radiation into a half-space (see Refs. 1–6 for an overview and references to the literature). For the planar transducer, the integration over the radiating aperture can in several cases explicitly be reduced to one over the rim of the aperture. Now, in the Kirchhoff theory of diffraction of light by an aperture in a black screen, it is known that for a whole class of aperture distributions one can show that the result of the surface integration over the aperture is only a functional of its rim, and for a number of cases the corresponding reduction from the surface integration to a line integration can indeed be carried out explicitly. In these cases, the Maggi–Rubinowicz transformation yields the tool to achieve this.[7–12] For our present purpose, this transformation (with a minor modification) also turns out to lead to the desired result. It is found that it not only applies to the planar transducer but also to the focused one with a spherical radiating aperture. Using the transformation, the transient acoustic pressure radiated from a focused (spherical) transducer with an arbitrary rim is expressed as a line integral over its rim. With the aid of the result, the transmitting properties of focused transducers can be studied. Numerical results are presented for the cases of a spherical-cap transducer and a spherically curved rectangular-strip transducer. They clearly show, directly in the time domain, the focusing properties of the transducers.

The so-called *impulse response method* for calculating the acoustic wave field radiated by a transducer is standardly based on the Rayleigh integral representation with a normal component of the particle velocity having a prescribed value on the plane bounding the half-space where the radiation is to be calculated. This representation reproduces the prescribed values and thus yields an exact solution to a *boundary-value problem* (for a half-space). The representation strictly loses its validity as soon as the surface on which the normal component of the particle velocity is prescribed deviates from a plane (such as is done for a focused transducer). Further, for a freely vibrating transducer (i.e., one without an infinite perfectly rigid baffle), the representation is incapable of evaluating the radiation in the half-space "behind" the transducer. The Kirchhoff–Huygens representation used in the present work, on the other hand, reproduces the prescribed jumps in the acoustic pressure and the normal component of the particle velocity across the radiating surface and thus presents an exact solution to a *saltus* problem (see Ref. 11). It applies to curved as well as planar transducers and gives the radiated wave field in all space, i.e., also behind the transducer. In this realm, our analysis, where the Kirchhoff–Huygens representation is rewritten in a computationally more advantageous form via the use of the Maggi–Rubinowicz transformation, is *exact*. The two approaches use different *Ansätze* and do yield different results, but we believe our approach to be the more consistent in case nonplanar and/or freely vibrating spherical radiators are involved. (For the related discussion with regard to the wave diffraction by disks and apertures in plane screens, see Bouwkamp.[13])

Finally, it should be remarked that the receiving properties of a focused transducer follow from the latter's transmitting properties by the combined proper application of the Rayleigh reciprocity theorem for acoustic wave fields and

[a]On leave from Delft University of Technology, Faculty of Electrical Engineering, Laboratory of Electromagnetic Research, P. O. Box 5031, 2600 GA Delft, The Netherlands. Telephone: +31-15785203; telefax +31-15783622.

 0001-4966/95/98(3)/1767/11/$6.00

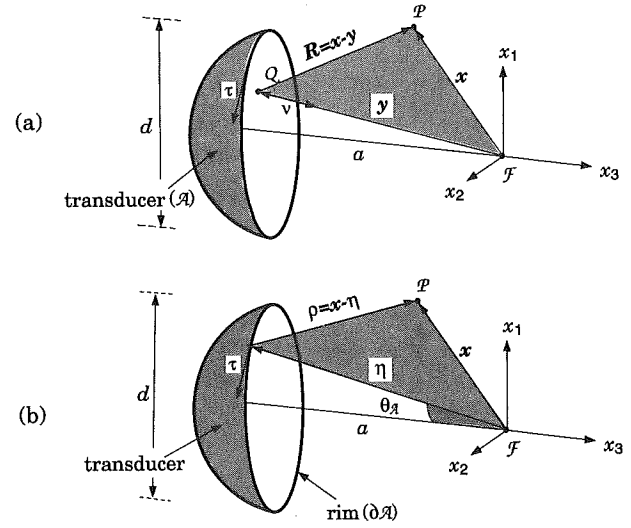

FIG. 1. (a) Geometry for radiating spherical surface $\mathscr{A}$. (b) Geometry for spherical-cap transducer. Relevant quantities are shown.

the Lorentz reciprocity theorem for electromagnetic fields.[14,15] As a consequence, the signal received from a point source at an arbitrary location can also be expressed in terms of a line integral over its rim.

I. DESCRIPTION OF THE CONFIGURATION AND THE KIRCHHOFF–HUYGENS REPRESENTATION FOR THE TRANSMITTED WAVE FIELD

The focused transducer consists of a radiating aperture $\mathscr{A}$ that forms part of a spherical surface of radius a and center $\mathscr{F}$ (focus). The transducer is immersed in an unbounded, homogeneous fluid with volume density of mass ρ, compressibility κ, and acoustic wave speed $c_f=(\kappa\rho)^{-1/2}$. The unit vector along the normal to $\mathscr{A}$ oriented toward the focus is denoted by $\boldsymbol{\nu}$. The oriented closed curve forming the rim of $\mathscr{A}$ is denoted by $\partial\mathscr{A}$. The unit vector along the tangent to $\partial\mathscr{A}$ is denoted by $\boldsymbol{\tau}$; $\boldsymbol{\nu}$ and $\boldsymbol{\tau}$ form a right-handed system. The focus of the transducer will be chosen as the origin of a right-handed, orthogonal, Cartesian coordinate system $\{x_1,x_2,x_3\}$ that is used to specify position in space. The position vector from $\mathscr{F}$ to an arbitrary point of observation $\mathscr{P}$ in the fluid is denoted by $\mathbf{x}$ and the one from $\mathscr{F}$ to a point $\mathscr{Q}$ on $\mathscr{A}$ is denoted by $\mathbf{y}$. Further, $\mathbf{R}=\mathbf{x}-\mathbf{y}$ is the vectorial distance from $\mathscr{Q}$ to $\mathscr{P}$. The vectorial spatial derivative is denoted by ∇ and the subscripts $\mathbf{x}$ and $\mathbf{y}$ on it are used to indicate differentiations with respect to the coordinates of $\mathscr{P}$ and $\mathscr{Q}$, respectively [Fig. 1(a)]. The time coordinate is t; differentiation with respect to t is denoted by ∂_t.

The acoustic pressure $p(\mathbf{x},t)$ of the radiated acoustic wave motion is calculated by starting from its Kirchhoff–Huygens representation in which suitable values of $p(\mathbf{y},t)$, its time derivative $\partial_t p(\mathbf{y},t)$, and its normal derivative $\boldsymbol{\nu}\cdot\nabla_{\mathbf{y}}p(\mathbf{y},t)$ on $\mathscr{A}$ are to be substituted. The relevant representation is given by

$$p(\mathbf{x},t)=\int_{\mathbf{y}\in\mathscr{A}}\left[-\boldsymbol{\nu}\cdot\nabla_{\mathbf{x}}\left(\frac{p(\mathbf{y},t-|\mathbf{R}|/c_f)}{4\pi|\mathbf{R}|}\right)-\frac{\boldsymbol{\nu}\cdot\nabla_{\mathbf{y}}p(\mathbf{y},t-|\mathbf{R}|/c_f)}{4\pi|\mathbf{R}|}\right]dA. \tag{1}$$

If now, the substituted values of p, $\partial_t p$, and $\boldsymbol{\nu}\cdot\nabla_{\mathbf{y}}p$ on $\mathscr{A}$ can be continued away from $\mathscr{A}$ such that they are compatible with an acoustic wave motion in the surrounding fluid, the result of the Kirchhoff–Huygens integration is not altered if the actual integration is carried out over a surface differing from $\mathscr{A}$, provided that the latter surface also has $\partial\mathscr{A}$ as its boundary curve, and in between the two surfaces the integrand is regular. Under these conditions, the expression for the acoustic pressure at the point of observation is a functional of the rim of the transducer only. Maggi[7] has pursued this idea in the theory of the Kirchhoff diffraction of light by an aperture in a black screen and he seems to have been the first to have carried out the transformation from surface integral to line integral explicitly for specific types of light sources. A different approach to the relevant transformation has been followed by Rubinowicz.[8] The corresponding derivations can be found in Baker and Copson[11] and in Rubinowicz.[8]

In our particular application the idea is to take the substituted values of p, $\partial_t p$, and $\boldsymbol{\nu}\cdot\nabla_{\mathbf{y}}p$ on $\mathscr{A}$ such that they are compatible with a spherical wave motion converging toward the focus $\mathscr{F}$ of the transducer. With this *Ansatz*, the transformation from the surface integration over $\mathscr{A}$ to a line integration along its rim $\partial\mathscr{A}$ can be carried out explicitly. In this procedure, proper care has to be taken of the occurrence of two singularities in the resulting integrand, viz., at $\mathscr{F}$ and at $\mathscr{P}$.

Although the entire analysis can be carried out in the space-time domain, we shall use the time Laplace transform domain analysis as an intermediate step. One reason for doing this is that some of the formula manipulations can be somewhat more easily carried out in this domain. On the other hand, for some applications the frequency-domain counterparts of the results may also be of interest and these follow from the time Laplace transform domain expressions upon replacing in the latter the transform parameter s by $j\omega$, where j is the imaginary unit and ω is the angular frequency of a frequency-domain constituent of the acoustic wave. We assume that the Huygens sources at $\mathscr{A}$ are active for $t>0$; then the time Laplace transform of the acoustic pressure that is causally related to them is given by

$$\hat{p}(\mathbf{x},s)=\int_{t=0}^{\infty}\exp(-st)p(\mathbf{x},t)dt,\quad \text{for}\quad s\in\mathscr{C}\ \text{with}\ \mathrm{Re}(s)>0. \tag{2}$$

Under this transformation, Eq. (1) transforms into the Helmholtz–Huygens representation

$$\hat{p}(\mathbf{x},s)=\int_{\mathbf{y}\in\mathscr{A}}[\hat{p}(\mathbf{y},s)\boldsymbol{\nu}\cdot\nabla_{\mathbf{y}}\hat{G}(\mathbf{x},\mathbf{y},s)-\hat{G}(\mathbf{x},\mathbf{y},s)\boldsymbol{\nu}\cdot\nabla_{\mathbf{y}}\hat{p}(\mathbf{y},s)]dA, \tag{3}$$

in which

$$\hat{G}(\mathbf{x},\mathbf{y},s)=\frac{\exp(-s|\mathbf{R}|/c_f)}{4\pi|\mathbf{R}|}, \tag{4}$$

and the property $\nabla_{\mathbf{x}}\hat{G}=-\nabla_{\mathbf{y}}\hat{G}$ has been used.

II. THE MAGGI–RUBINOWICZ LINE INTEGRAL REPRESENTATION FOR THE TRANSMITTED ACOUSTIC WAVE FIELD

To model the action of the focused transducer with a spherically curved radiating surface of radius a and center at $\mathscr{F}$, we substitute in Eq. (3) for the acoustic pressure and its normal derivative on $\mathscr{A}$ given values that are compatible with a spherical wave motion converging toward $\mathscr{F}$. The time Laplace transform of the acoustic pressure of the latter is taken as

$$\hat{p}_0(\mathbf{y},s)=\hat{P}_0(s)\,\frac{\exp[s(|\mathbf{y}|-a)/c_f]}{|\mathbf{y}|/a}, \tag{5}$$

where $\hat{P}_0(s)$ is the time Laplace transform of the value of the acoustic pressure $P_0(t)$ at the transducer's surface $|\mathbf{y}|=a$. The gradient of this expression follows as (note that $\boldsymbol{\nu}=-\mathbf{y}/|\mathbf{y}|$ on $\mathscr{A}$)

$$\nabla_{\mathbf{y}}\hat{p}_0=\hat{P}_0(s)\left(\frac{s}{c_f}-\frac{1}{|\mathbf{y}|}\right)\frac{\exp[s(|\mathbf{y}|-a)/c_f]}{|\mathbf{y}|/a}\,\frac{\mathbf{y}}{|\mathbf{y}|}. \tag{6}$$

With this, the values of the acoustic pressure and its normal derivative at the transducer surface follow as

$$\hat{p}=\hat{P}_0(s), \quad \text{at } |\mathbf{y}|=a, \tag{7}$$

$$\boldsymbol{\nu}\cdot\nabla_{\mathbf{y}}\hat{p}=-\left(\frac{s}{c_f}-\frac{1}{a}\right)\hat{P}_0(s), \quad \text{at } |\mathbf{y}|=a. \tag{8}$$

To transform the resulting integral over $\mathscr{A}$ at the right-hand side of Eq. (3) into a line integral over $\partial\mathscr{A}$, the surface of integration is tentatively deformed into a cone $\mathscr{K}$ that has $\partial\mathscr{A}$ as its directrix and $\mathscr{F}$ as its apex. In this procedure, the singularity in $\hat{p}_0$ and $\nabla_{\mathbf{y}}\hat{p}_0$ at $\mathscr{F}$ is excluded by the sphere $\mathscr{S}_\delta$ of arbitrarily small radius δ around $\mathscr{F}$. In the limit $\delta\to 0$, the contribution from $\mathscr{S}_\delta$ is found to be

$$\lim_{\delta\to 0}\int_{\mathbf{y}\in\mathscr{S}_\delta}[\hat{p}_0(\mathbf{y},s)\boldsymbol{\nu}\cdot\nabla_{\mathbf{y}}\hat{G}(\mathbf{x},\mathbf{y},s) - \hat{G}(\mathbf{x},\mathbf{y},s)\boldsymbol{\nu}\cdot\nabla_{\mathbf{y}}\hat{p}_0(\mathbf{y},s)]dA = -\frac{\Omega_{\mathscr{A}}}{4\pi}\hat{P}_0(s)\,\frac{\exp[-s(|\mathbf{x}|+a)/c_f]}{|\mathbf{x}|/a}, \quad \text{for } |\mathbf{x}|\neq 0, \tag{9}$$

where $\Omega_{\mathscr{A}}$ is the solid angle under which $\mathscr{A}$ is viewed upon from $\mathscr{F}$. Along $\mathscr{K}$, we have $\boldsymbol{\nu}\cdot\mathbf{y}=0$ and hence $\boldsymbol{\nu}\cdot\nabla_{\mathbf{y}}\hat{p}_0=0$. To evaluate the remaining integral along $\mathscr{K}$, a system of oblique conical coordinates is introduced consisting of the straight lines (generators) from $\mathscr{F}$ to any point on $\partial\mathscr{A}$ and the closed curves that arise from $\partial\mathscr{A}$ by multiplying the distance from $\mathscr{F}$ to any point on $\partial\mathscr{A}$ by a factor of λ, with $\delta\leq\lambda\leq 1$. Indicating the position vector from $\mathscr{F}$ to any point on $\partial\mathscr{A}$ by $\boldsymbol{\eta}$ and the position vector from $\boldsymbol{\eta}$ to the point of observation $\mathbf{x}$ by $\boldsymbol{\rho}$, we have

$$\mathbf{y}=\lambda\boldsymbol{\eta}, \quad \text{for } \mathbf{y}\in\mathscr{K}, \tag{10}$$

$$\mathbf{R}=\mathbf{x}-\lambda\boldsymbol{\eta}, \quad \text{for } \mathbf{y}\in\mathscr{K}, \tag{11}$$

while the vectorial elementary surface area on $\mathscr{K}$ is given by

$$\boldsymbol{\nu}\,dA=d\mathbf{y}\times\lambda\boldsymbol{\tau}\,d\sigma=\boldsymbol{\eta}\,d\lambda\times\lambda\boldsymbol{\tau}\,d\sigma, \quad \text{for } \mathbf{y}\in\mathscr{K}, \tag{12}$$

where $d\sigma$ is the elementary arc length along $\partial\mathscr{A}$. With this, the remaining integral over $\mathscr{K}$ becomes

$$\int_{\mathbf{y}\in\mathscr{K}}\hat{p}_0(\mathbf{y},s)\boldsymbol{\nu}\cdot\nabla_{\mathbf{y}}\hat{G}(\mathbf{x},\mathbf{y},s)dA = \lim_{\delta\to 0}\hat{P}_0(s)\int_{\boldsymbol{\eta}\in\partial\mathscr{A}}(\boldsymbol{\eta}\times\boldsymbol{\tau})d\sigma \times\int_{\lambda=\delta}^{1}\frac{\exp(s\lambda|\boldsymbol{\eta}|/c_f-sa/c_f)}{\lambda|\boldsymbol{\eta}|/a}\left(\frac{s}{c_f}+\frac{1}{|\mathbf{R}|}\right) \times\frac{\mathbf{R}}{|\mathbf{R}|}\,\frac{\exp(-s|\mathbf{R}|/c_f)}{4\pi|\mathbf{R}|}\,\lambda\,d\lambda, \tag{13}$$

in which

$$|\mathbf{R}|=[(\lambda\boldsymbol{\eta}-\mathbf{x})\cdot(\lambda\boldsymbol{\eta}-\mathbf{x})]^{1/2}\geq 0. \tag{14}$$

In the right-hand side of Eq. (13) the limit $\delta\to 0$ can be taken by just replacing the lower limit δ of the integration with respect to λ by zero, provided that $|\mathbf{x}|\neq 0$. Further, we use the fact that [cf. Eq. (11)] $(\boldsymbol{\eta}\times\boldsymbol{\tau})\cdot\mathbf{R}=(\mathbf{x}\times\boldsymbol{\eta})\cdot\boldsymbol{\tau}$. Now, by straightforward differentiation, it can be verified that

$$\frac{\partial}{\partial\lambda}\left[\frac{\exp(s\lambda|\boldsymbol{\eta}|/c_f-s|\mathbf{R}|/c_f)}{|\mathbf{R}|(|\boldsymbol{\eta}||\mathbf{R}|+\boldsymbol{\eta}\cdot\mathbf{R})}\right] =\left(\frac{s}{c_f}+\frac{1}{|\mathbf{R}|}\right)\frac{\exp(s\lambda|\boldsymbol{\eta}|/c_f-s|\mathbf{R}|/c_f)}{|\mathbf{R}|^2}, \tag{15}$$

where the relation

$$|\mathbf{R}|\,\frac{\partial|\mathbf{R}|}{\partial\lambda}=-\boldsymbol{\eta}\cdot\mathbf{R} \tag{16}$$

has been used. Putting things together, we arrive at

$$\hat{p}(\mathbf{x},s)=-\frac{\Omega_{\mathscr{A}}}{4\pi}\hat{P}_0(s)\,\frac{\exp[-s(|\mathbf{x}|+a)/c_f]}{|\mathbf{x}|/a}+\frac{\hat{P}_0(s)}{4\pi} \times\int_{\boldsymbol{\eta}\in\partial\mathscr{A}}\left[\frac{\exp(-s|\boldsymbol{\rho}|/c_f)}{|\boldsymbol{\rho}|(a|\boldsymbol{\rho}|+\boldsymbol{\eta}\cdot\boldsymbol{\rho})}-\frac{\exp[-s(|\mathbf{x}|+a)/c_f]}{|\mathbf{x}|(a|\mathbf{x}|+\boldsymbol{\eta}\cdot\mathbf{x})}\right] \times(\boldsymbol{\rho}\times\mathbf{x})\cdot\boldsymbol{\tau}\,d\sigma \quad \text{for } |\mathbf{x}|\neq 0, \tag{17}$$

in which $\boldsymbol{\rho}=\mathbf{x}-\boldsymbol{\eta}$ is the vectorial distance from a point of integration $\boldsymbol{\eta}$ on $\partial\mathscr{A}$ to a point of observation $\mathbf{x}$ and where we have taken into account that $|\boldsymbol{\eta}|=a$ [Fig. 1(b)].

The right-hand side of Eq. (17) yields the expression for the acoustic wave field radiated by the transducer as long as the point $\mathscr{P}$ of observation is located outside the domain bounded by $\mathscr{A}$ and $\mathscr{K}$. For points of observation located inside this domain, the contribution from the singularity of $\hat{G}$ at $\mathscr{P}$ has to be taken into account. This is done in the standard manner by surrounding $\mathscr{P}$ by a sphere of vanishingly small radius and calculating the contribution from this sphere upon letting its radius go to zero. The result is then

$$\hat{p}(\mathbf{x},s)=\hat{p}_0(\mathbf{x},s) + \text{right-hand side of Eq. (17)}, \quad \text{for } |\mathbf{x}|\neq 0. \tag{18}$$

When $\mathscr{P}$ is located on $\mathscr{K}$, i.e., on one of straight lines joining the focus $\mathscr{F}$ with the rim $\partial\mathscr{A}$, the acoustic wave field is given by

$$\hat{p}(\mathbf{x},s)=\tfrac{1}{2}\hat{p}_0(\mathbf{x},s)+\text{principal value of right-hand side of Eq. (17), for } |\mathbf{x}|\neq 0. \tag{19}$$

Equations (17)–(19) provide the Maggi–Rubinowicz line integral representations for the transmitted acoustic wave field in the time Laplace transform domain. The corresponding *frequency-domain* results for an exponential time factor $\exp(j\omega t)$ are obtained by replacing in the right-hand sides of Eqs. (17)–(19) the time Laplace transform parameter s by $j\omega$.

The *time-domain* results are obtained by applying to the right-hand sides of Eqs. (17)–(19) the shift rule of the Laplace transformation:

$$\hat{P}_0(s)\exp(-sT)\rightarrow P_0(t-T), \tag{20}$$

where T is a time delay. The application of this rule to Eq. (17) leads to

$$p(\mathbf{x},t)=-\frac{\Omega_{\mathscr{A}}}{4\pi}\frac{P_0[t-(|\mathbf{x}|+a)/c_f]}{|\mathbf{x}|/a}+\frac{1}{4\pi}\int_{\boldsymbol{\eta}\in\partial\mathscr{A}}\left(\frac{P_0[t-|\boldsymbol{\rho}|/c_f]}{|\boldsymbol{\rho}|(a|\boldsymbol{\rho}|+\boldsymbol{\eta}\cdot\boldsymbol{\rho})}-\frac{P_0[t-(|\mathbf{x}|+a)/c_f]}{|\mathbf{x}|(a|\mathbf{x}|+\boldsymbol{\eta}\cdot\mathbf{x})}\right)(\boldsymbol{\rho}\times\mathbf{x})\cdot\boldsymbol{\tau}\,d\sigma \quad \text{for } |\mathbf{x}|\neq 0, \tag{21}$$

while Eqs. (18) and (19) transform into

$$p(\mathbf{x},t)=p_0(\mathbf{x},t)+\text{right-hand side of Eq. (21) for } |\mathbf{x}|\neq 0 \tag{22}$$

and

$$p(\mathbf{x},t)=\tfrac{1}{2}p_0(\mathbf{x},t)+\text{principal value of right-hand side of Eq. (21) for } |\mathbf{x}|\neq 0, \tag{23}$$

respectively. Note that in the time-domain expressions only causal contributions occur since in all terms in our representation the time delay is non-negative.

For the final evaluation of the acoustic wave field, a simple, one-dimensional integral over the rim $\partial\mathscr{A}$ of the radiating aperture $\mathscr{A}$ remains to be evaluated. In general, this integration has to carried out numerically. In our expressions, the position of the rim is most naturally expressed through its parametric representation, where the Cartesian components of $\boldsymbol{\eta}$ are given functions of the arc length σ along the rim. In this form, the evaluation goes through for arbitrary shapes of the rim.

For arbitrary shapes of the rim, the value of $\Omega_{\mathscr{A}}$ will also have to be determined numerically. For this, the expression

$$\Omega_{\mathscr{A}}=-\int_{\mathbf{y}\in\mathscr{A}}\frac{\boldsymbol{\nu}\cdot\boldsymbol{\eta}}{|\mathbf{y}|^3}\,dA=\int_{\mathbf{y}\in\mathscr{A}}\frac{dA}{|\mathbf{y}|^2} \tag{24}$$

can be used, in which $|\mathbf{y}|=a$.

It is tempting to interpret the different contributions at the right-hand side of Eq. (21) on the basis of their travel times. The first line integral can then be considered as the superposition of the contributions from the elementary parts of the rim of the transducer. The first term on the right-hand side and the second integral contain contributions with the travel time $(|\mathbf{x}|+a)/c_f$, which is the travel time from the point diametrically opposite (antipodal) to the projection of the point of observation $\mathscr{P}$ on the sphere of which the transducer forms a part, with $\mathscr{F}$ as center. In this interpretation one has to realize, however, that the complete expression quantifies the totality of the diffraction phenomena associated with the boundedness of the radiating surface of the transducer and that each constituent does not necessarily represent an isolated phenomenon.

A. The acoustic wave field at the focus

The acoustic wave field at the focus is found by straightforward evaluation of Eq. (3), after having substituted Eqs. (5) and (6). We obtain

$$\hat{p}(\mathbf{0},s)=\frac{\Omega_{\mathscr{A}}}{4\pi}\frac{2sa}{c_f}\hat{P}_0(s)\exp\left(-\frac{sa}{c_f}\right). \tag{25}$$

The corresponding time-domain result is

$$p(\mathbf{0},t)=\frac{\Omega_{\mathscr{A}}}{4\pi}\frac{2a}{c_f}\partial_t P_0\left(t-\frac{a}{c_f}\right), \tag{26}$$

where the property $s\rightarrow\partial_t$ has been used. Note that in the right-hand side of Eq. (26) the time derivative of the pulse shape $P_0(t)$ occurs, whereas Eqs. (21)–(23) consist of superpositions of properly weighted and retarded actual pulse shapes distributed over $\partial\mathscr{A}$. A similar result worked out for a focused transducer with a circular rim has been derived in Ref. 4. Here, it is expressed in terms of the solid angle under which the transducer surface of arbitrary rim is viewed from the focus.

B. Acoustic wave field expressions in terms of the particle velocity at the transducer's surface

So far, the radiated acoustic wave field has been expressed in terms of the value of the acoustic pressure $\hat{P}_0(s)$, or $P_0(t)$, at the transducer's surface. This pressure is related to the normal component (along $\boldsymbol{\nu}$) of the particle velocity $\hat{V}_0(s)$, or $V_0(t)$, on this surface via (note that the corresponding wave motion is converging towards $\mathscr{F}$)

$$\hat{V}_0(s)=\frac{1}{\rho s}\left(\frac{s}{c_f}-\frac{1}{a}\right)\hat{P}_0(s) \tag{27}$$

or

$$\hat{P}_0(s)=\rho c_f\left[1+\frac{1}{a}\left(\frac{s}{c_f}-\frac{1}{a}\right)^{-1}\right]\hat{V}_0(s). \tag{28}$$

The time-domain counterpart of the latter expression is

$$P_0(t)=\rho c_f\left[V_0(t)+\frac{c_f}{a}\times\int_{t'=0}^{t}\exp\left(\frac{c_f(t-t')}{a}\right)V_0(t')dt'\right]. \tag{29}$$

III. ALTERNATIVE EVALUATION OF THE KIRCHHOFF–HUYGENS SURFACE INTEGRAL

An alternative reduction of the two-dimensional Kirchhoff–Huygens surface integral to a one-dimensional one is obtained by proceeding along the lines that Faure *et al.*[6] have followed in the evaluation of a Rayleigh integral applied to a curved transducer mounted in an infinite rigid baffle. For our case, this method consists of first introducing a spherical coordinate system $\{a,\theta,\phi\}$ for points on the transducer's surface with the polar axis along the line from $\mathscr{F}$ to $\mathscr{P}$ and ranges of integration that are a subset of $\{0\leqslant\theta\leqslant\pi,0\leqslant\phi<2\pi\}$. Then,

$$|\mathbf{R}|^2=|\mathbf{x}|^2+a^2-2|\mathbf{x}|a\cos(\theta). \tag{30}$$

Using this equation to introduce $|\mathbf{R}|$ instead of θ as a variable of integration, we have

$$|\mathbf{R}|d|\mathbf{R}|=|\mathbf{x}|a\sin(\theta)d\theta \tag{31}$$

and

$$dA=a^2\sin(\theta)d\theta\,d\phi=\frac{a|\mathbf{R}|}{|\mathbf{x}|}d|\mathbf{R}|d\phi. \tag{32}$$

Now, for the integrand at hand, the integration with respect to $|\mathbf{R}|$ at fixed ϕ can be carried out explicitly. The different steps for this are given below.

In the first term on the right-hand side of Eq. (3) we need the result

$$\boldsymbol{\nu}\cdot\nabla_{\mathbf{y}}\hat{G}=(\partial_{|\mathbf{R}|}\hat{G})\boldsymbol{\nu}\cdot(-\mathbf{R}/|\mathbf{R}|)=(-\partial_{|\mathbf{R}|}\hat{G})\frac{|\mathbf{R}|^2+a^2-|\mathbf{x}|^2}{2a|\mathbf{R}|}. \tag{33}$$

Integration by parts then yields

$$\int_{|\mathbf{R}|_{\min}}^{|\mathbf{R}|_{\max}}\boldsymbol{\nu}\cdot\nabla_{\mathbf{y}}\hat{G}a^2\sin(\theta)d\theta=\int_{|\mathbf{R}|_{\min}}^{|\mathbf{R}|_{\max}}\boldsymbol{\nu}\cdot\nabla_{\mathbf{y}}\hat{G}\frac{a|\mathbf{R}|}{|\mathbf{x}|}d|\mathbf{R}|=\frac{1}{2|\mathbf{x}|}[-\hat{G}(|\mathbf{R}|^2+a^2-|\mathbf{x}|^2)]_{|\mathbf{R}|_{\min}}^{|\mathbf{R}|_{\max}}+\frac{1}{|\mathbf{x}|}\int_{|\mathbf{R}|_{\min}}^{|\mathbf{R}|_{\max}}\hat{G}|\mathbf{R}|d|\mathbf{R}|, \tag{34}$$

where $|\mathbf{R}|_{\min}$ is the value of $|\mathbf{R}|$ at the minimum value $\theta_{\min}$ of θ and $|\mathbf{R}|_{\max}$ is the value of $|\mathbf{R}|$ at the maximum value $\theta_{\max}$ of θ in the range of the integration with respect to θ.

For the second term on the right-hand side of Eq. (3) we need the result

$$\frac{s}{c_f}\int_{|\mathbf{R}|_{\min}}^{|\mathbf{R}|_{\max}}\hat{G}a^2\sin(\theta)d\theta=\frac{s}{c_f}\int_{|\mathbf{R}|_{\min}}^{|\mathbf{R}|_{\max}}\hat{G}\frac{a|\mathbf{R}|}{|\mathbf{x}|}d|\mathbf{R}|=\frac{a}{4\pi|\mathbf{x}|}[-\exp(-s|\mathbf{R}|/c_f)]_{|\mathbf{R}|_{\min}}^{|\mathbf{R}|_{\max}}. \tag{35}$$

Putting things together, we end up with the expression

$$\hat{p}(\mathbf{x},s)=\frac{\hat{P}_0(s)}{2|\mathbf{x}|}\int_{\phi_{\min}}^{\phi_{\max}}\left(-[(|\mathbf{R}|+a)^2-|\mathbf{x}|^2]\times\frac{\exp(-s|\mathbf{R}|/c_f)}{4\pi|\mathbf{R}|}\right)_{|\mathbf{R}|=|\mathbf{R}|_{\min}(\phi)}^{|\mathbf{R}|_{\max}(\phi)}d\phi,\quad\text{for } |\mathbf{x}|\neq 0. \tag{36}$$

where the ranges of integration follow from the specification of the rim of the transducer's radiating surface. For Eq. (36) to hold, the range of integration in Eq. (3) must, if necessary, be subdivided into parts for which the mapping from $\mathbf{y}$ on $|\mathbf{y}|=a$ to θ and ϕ as variables of integration is one-to-one. This subdivision depends on the location of the point of observation.

The time-domain counterpart of Eq. (36) is

$$p(\mathbf{x},t)=\frac{1}{2|\mathbf{x}|}\int_{\phi_{\min}}^{\phi_{\max}}\left(-[(|\mathbf{R}|+a)^2-|\mathbf{x}|^2]\times\frac{P_0(t-|\mathbf{R}|/c_f)}{4\pi|\mathbf{R}|}\right)_{|\mathbf{R}|_{\min}(\phi)}^{|\mathbf{R}|_{\max}(\phi)}d\phi\quad\text{for } |\mathbf{x}|\neq 0. \tag{37}$$

In practice, the whole procedure can only be carried out for rims whose specification allows for an analytical expressions for $|\mathbf{R}|_{\min}(\phi)$ and $|\mathbf{R}|_{\max}(\phi)$, as well as $\phi_{\min}$ and $\phi_{\max}$. For this reason we have based our further computations on the more general result given in Sec. II.

IV. THE WAVE FIELD TRANSMITTED BY A SPHERICAL-CAP TRANSDUCER

In this section we present the results for a focused transducer as considered in Sec. I in the case where the rim is a circle of diameter $d<2a$ (spherical-cap transducer). The semiangle $\theta_{\mathscr{R}}$ included at the apex of the circular cone with $\mathscr{F}$ as its center and the rim as its directrix is then given through

$$\sin(\theta_{\mathscr{R}})=d/2a. \tag{38}$$

It is assumed that $\theta_{\mathscr{R}}\leqslant\pi/2$. Then

$$\cos(\theta_{\mathscr{R}})=[1-(d/2a)^2]^{1/2}. \tag{39}$$

First, we evaluate the solid angle $\Omega_{\mathscr{R}}$. Introducing the angle θ included between the axis of symmetry of the transducer and the position vector from the focus to a point of integration on the transducer's surface as the variable of integration, we obtain

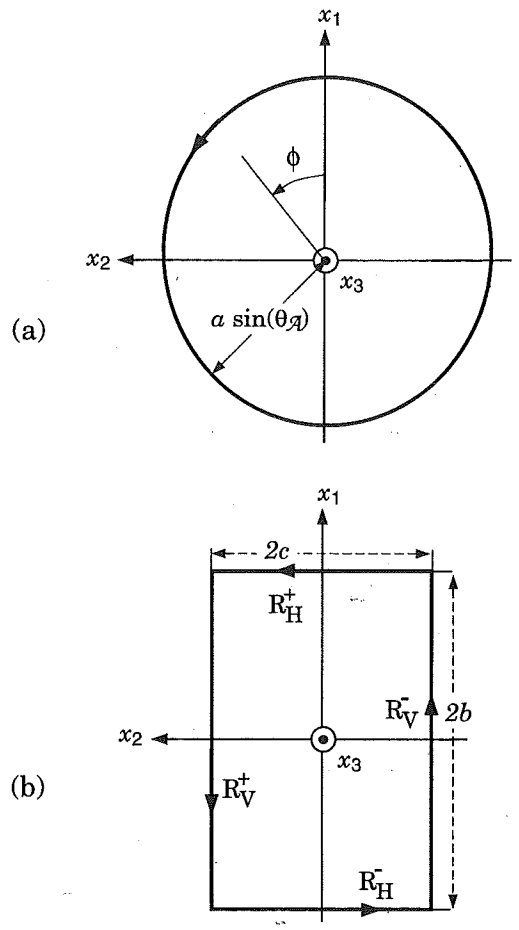

FIG. 2. (a) Circular rim for spherical-cap transducer. (b) Projection of spherically curved rectangular-strip transducer showing horizontal ($R_H^{\pm}$) and vertical ($R_V^{\pm}$) strips of rim.

$$\Omega_{\mathscr{A}}=2\pi\int_{\theta=0}^{\theta_{\mathscr{A}}}\sin(\theta)d\theta=2\pi[1-\cos(\theta_{\mathscr{A}})]. \tag{40}$$

To carry out the integration along the rim of the aperture, we employ polar coordinates in the plane of the circular rim. Since the transmitted wave field is rotationally symmetric around the axis of the transducer, we can without loss of generality take the point of observation in the x_1, x_3 plane. Correspondingly, let the point of observation (position vector $\mathbf{x}$) have the Cartesian corodinates $\{X,0,Z\}$ and let the Cartesian coordinates of an integration point (position vector $\boldsymbol{\eta}$) be $\{a\sin(\theta_{\mathscr{A}})\cos(\phi),a\sin(\theta_{\mathscr{A}})\sin(\phi),-a\cos(\theta_{\mathscr{A}})\}$; then [Fig. 2(a)]

$$\int_{\boldsymbol{\eta}\in\partial\mathscr{A}}\cdots d\sigma=a\sin(\theta_{\mathscr{A}})\int_{\phi=0}^{2\pi}\cdots d\phi, \tag{41}$$

while

$$|\boldsymbol{\rho}|=\{[X-a\sin(\theta_{\mathscr{A}})\cos(\phi)]^2+a^2\sin^2(\theta_{\mathscr{A}})\sin^2(\phi)+[Z+a\cos(\theta_{\mathscr{A}})]^2\}^{1/2}, \tag{42}$$

$$\boldsymbol{\eta}\cdot\boldsymbol{\rho}=\boldsymbol{\eta}\cdot\mathbf{x}-\boldsymbol{\eta}\cdot\boldsymbol{\eta}=Xa\sin(\theta_{\mathscr{A}})\cos(\phi)-Za\cos(\theta_{\mathscr{A}})-a^2, \tag{43}$$

$$|\mathbf{x}|=(X^2+Z^2)^{1/2}, \tag{44}$$

$$\boldsymbol{\eta}\cdot\mathbf{x}=Xa\sin(\theta_{\mathscr{A}})\cos(\phi)-Za\cos(\theta_{\mathscr{A}}), \tag{45}$$

$$\mathbf{x}\times\boldsymbol{\eta}\cdot\boldsymbol{\tau}=Xa\cos(\phi)\cos(\theta_{\mathscr{A}})+Za\sin(\theta_{\mathscr{A}}). \tag{46}$$

Using these expressions in the right-hand sides of Eqs. (17)–(19), the integration with respect to ϕ is to be carried out numerically. As a check on the accuracy of the result, we can use the expressions for the transmitted wave field on the axis of the transducer. This wave field can be determined explicitly, from both the Kirchhoff–Huygens representation over the surface of the transducer and from the line integral representation along the rim of the transducer, and therefore yields in itself a check on the whole procedure of transforming the surface integral into a line integral.

A. The transmitted acoustic wave field on the axis of the transducer

1. Evaluation of the Kirchhoff–Huygens integral

The Kirchhoff–Huygens integral is evaluated by using the polar angles ϕ and θ as the variables of integration. Then, $\mathbf{x}=\{0,0,Z\}$, $\mathbf{y}=-a\boldsymbol{\nu}$, with $\boldsymbol{\nu}=\{-\sin(\theta)\cos(\phi),-\sin(\theta)\sin(\phi),\cos(\theta)\}$, and $\mathbf{R}=\{-a\sin(\theta)\cos(\phi),-a\sin(\theta)\times\sin(\phi),Z+a\cos(\theta)\}$. Hence

$$\boldsymbol{\nu}\cdot\mathbf{R}=a+Z\cos(\theta), \tag{47}$$

$$|\mathbf{R}|=[Z^2+2Za\cos(\theta)+a^2]^{1/2}, \tag{48}$$

$$\frac{\partial|\mathbf{R}|}{\partial\theta}=-\frac{Za\sin(\theta)}{|\mathbf{R}|}. \tag{49}$$

Introducing in the resulting integrals $|\mathbf{R}|$ as the variable of integration and carrying out the integrations, we obtain

$$p(0,0,Z,t)=\frac{(R_r+a)^2-Z^2}{4ZR_r}P_0\left(t-\frac{R_r}{c_f}\right)-\frac{a}{Z}\times P_0(t-R_c/c_f)H(Z+a)\quad\text{for } Z\neq 0, \tag{50}$$

where H denotes the Heaviside unit step function,

$$R_r=[Z^2+2Za\cos(\theta_{\mathscr{A}})+a^2]^{1/2} \tag{51}$$

is the distance from the rim to the on-axis point of observation, and

$$R_c=|Z+a| \tag{52}$$

is the distance from the center of the transducer surface to the on-axis point of observation. Note that at $Z=-a$ the second term on the right-hand side is discontinuous and reproduces the jumps across the surface of the transducer in the acoustic pressure and its normal derivative from zero to the values prescribed by Eqs. (7) and (8), a reproduction which is in accordance with the Kirchhoff theory of diffraction and that for $Z<-a$, i.e., behind the transducer, the second term on the right-hand side yields a vanishing contribution, which implies that the entire diffraction phenomenon is attributable to the rim.

As $Z\to 0$ (i.e., at the focus of the transducer), the limiting behavior follows from Eq. (50) as

$$p(0,0,0,t)=(a/c_f)[1-\cos(\theta_{\mathscr{H}})]\partial_t P_0(t-a/c_f), \quad (53)$$

which, in view of Eq. (40), is in accordance with the general result of Eq. (26).

2. Evaluation of the integral along the rim

Using in Eqs. (21)–(23) the values for the quantities listed in Eqs. (42)–(46) for $X=0$ and recalling that the resulting integrand is independent of ϕ, Eq. (50) is again arrived at.

3. Alternative evaluation of the Kirchhoff–Huygens integral

Also, evaluation of Eq. (37) leads to Eq. (50).

V. THE WAVE FIELD EMITTED BY A SPHERICALLY CURVED RECTANGULAR-STRIP TRANSDUCER

The spherically curved rectangular-strip transducer has a radiating surface whose projection on a plane perpendicular to the axis of the transducer has the shape of a rectangle. The dimensions of this rectangle are taken to be $2b$ in the x_1 direction and $2c$ in the x_2 direction. Its rim then consists of the following two "horizontal" circular arcs [Fig. 2(b)]:

$$\eta_1=\pm b, \quad \eta_2^2+\eta_3^2=a^2-b^2 \quad (54)$$

and the two "vertical" circular arcs

$$\eta_2=\pm c, \quad \eta_1^2+\eta_3^2=a^2-c^2, \quad (55)$$

and its four corners are

$$\eta_1=\pm b, \quad \eta_2=\pm c, \quad \eta_3=-(a^2-b^2-c^2)^{1/2}. \quad (56)$$

For the strip to exist, the condition $b^2+c^2<a^2$ must be satisfied. A similar geometry has been investigated in Ref. 6.

To carry out the integration along the rim, the circular arcs in the four planes that bound the rectangular strip are parameterized by introducing an angular polar variable in each of the two planes. For the "upper horizontal" circular arc we take

$$\eta_1=b,$$

$$\eta_2=(a^2-b^2)^{1/2}\sin(\phi_H), \quad (57)$$

$$\eta_3=-(a^2-b^2)^{1/2}\cos(\phi_H),$$

$$\text{for } -\alpha_H<\phi_H<\alpha_H,$$

with

$$\alpha_H=\sin^{-1}[c/(a^2-b^2)^{1/2}], \quad (58)$$

in terms of which

$$\boldsymbol{\tau}=\{0,\cos(\phi_H),\sin(\phi_H)\}. \quad (59)$$

For the "lower horizontal" circular arc we take

$$\eta_1=-b,$$

$$\eta_2=-(a^2-b^2)^{1/2}\sin(\phi_H), \quad (60)$$

$$\eta_3=-(a^2-b^2)^{1/2}\cos(\phi_H),$$

$$\text{for } -\alpha_H<\phi_H<\alpha_H,$$

with

$$\alpha_H=\sin^{-1}[c/(a^2-b^2)^{1/2}], \quad (61)$$

in terms of which

$$\boldsymbol{\tau}=\{0,-\cos(\phi_H),\sin(\phi_H)\}. \quad (62)$$

For the "front vertical" circular arc we take

$$\eta_1=-(a^2-c^2)^{1/2}\sin(\phi_V),$$

$$\eta_2=c, \quad (63)$$

$$\eta_3=-(a^2-c^2)^{1/2}\cos(\phi_V),$$

$$\text{for } -\alpha_V<\phi_V<\alpha_V,$$

with

$$\alpha_V=\sin^{-1}[b/(a^2-c^2)^{1/2}], \quad (64)$$

in terms of which

$$\boldsymbol{\tau}=\{-\cos(\phi_V),0,\sin(\phi_V)\}. \quad (65)$$

For the "rear vertical" circular arc we take

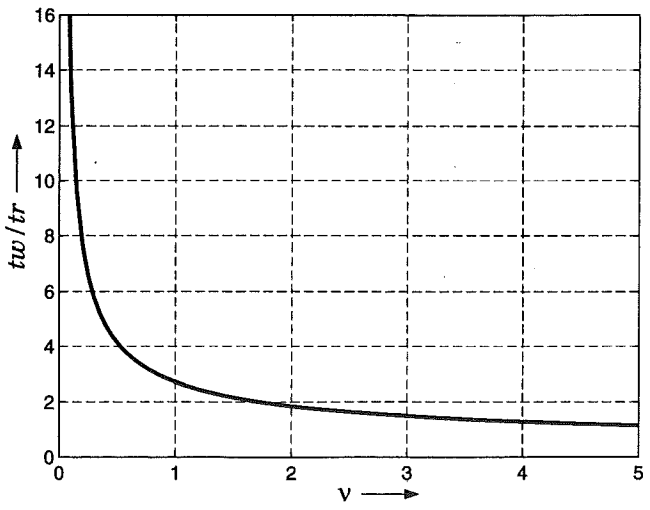

FIG. 3. Plot of t_w/t_r as a function of ν as given in Eq. (75).

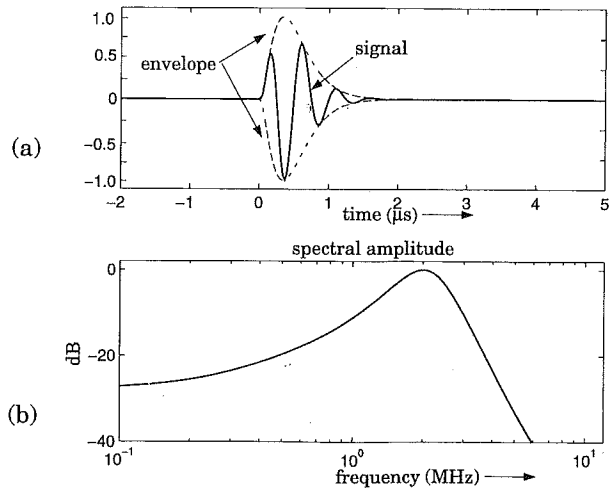

FIG. 4. (a) Signal and (b) corresponding spectral amplitude used for numerical results. Parameters: $f_0=2$ MHz, $\nu=2$, $\alpha=5.71\times10^6$ s^{-1}. Corresponding rise time and time width: $t_r=0.35$ μs, $t_w=0.65$ μs.

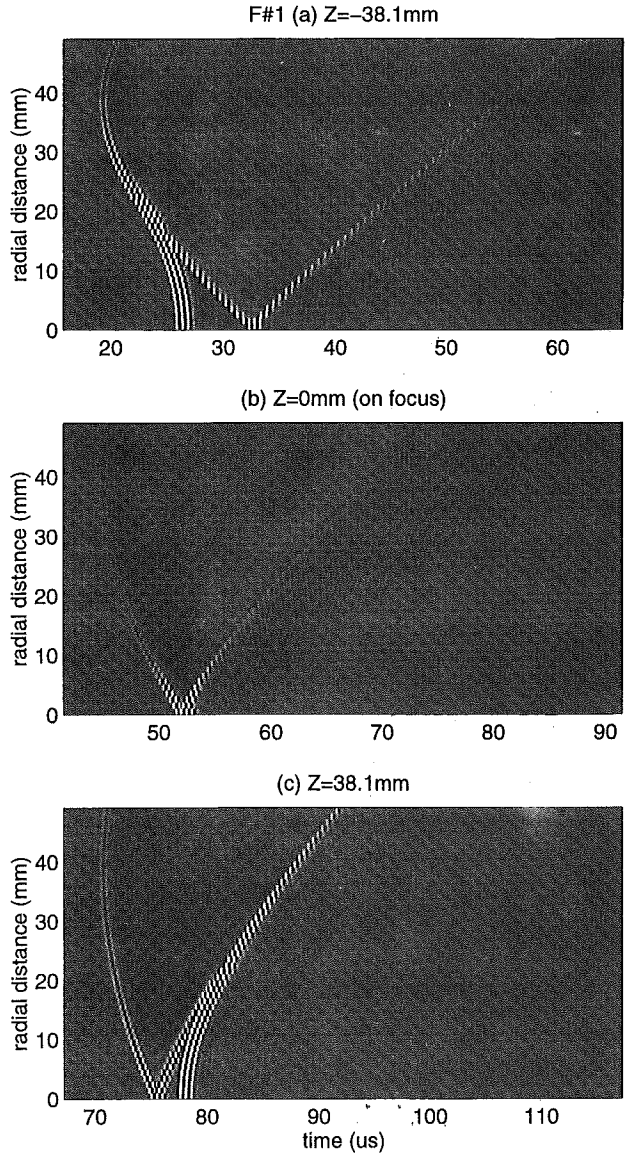

FIG. 5. Gray-scale image of amplitude of radiated signal from circular rim transducer, as a function of time and radial distance at three different ranges from aperture; Z indicates range along aperture axis. Parameters: $a=76.2$ mm, $d=76.2$ mm ($F/1$: this pertains to a strongly focusing transducer). Numerical noise shown as tails to arrivals is due to high saturation of the images introduced to highlight radial moveout of signal. Note that different time windows and amplitude scales are used in these figures.

$$\eta_1=(a^2-c^2)^{1/2}\sin(\phi_V),$$
$$\eta_2=-c, \tag{66}$$
$$\eta_3=-(a^2-c^2)^{1/2}\cos(\phi_V),$$
$$\text{for}-\alpha_V<\phi_V<\alpha_V,$$

with

$$\alpha_V=\sin^{-1}[b/(a^2-c^2)^{1/2}], \tag{67}$$

in terms of which

$$\boldsymbol{\tau}=\{\cos(\phi_V),0,\sin(\phi_V)\}. \tag{68}$$

The solid angle $\Omega_{\mathscr{A}}$ is given by

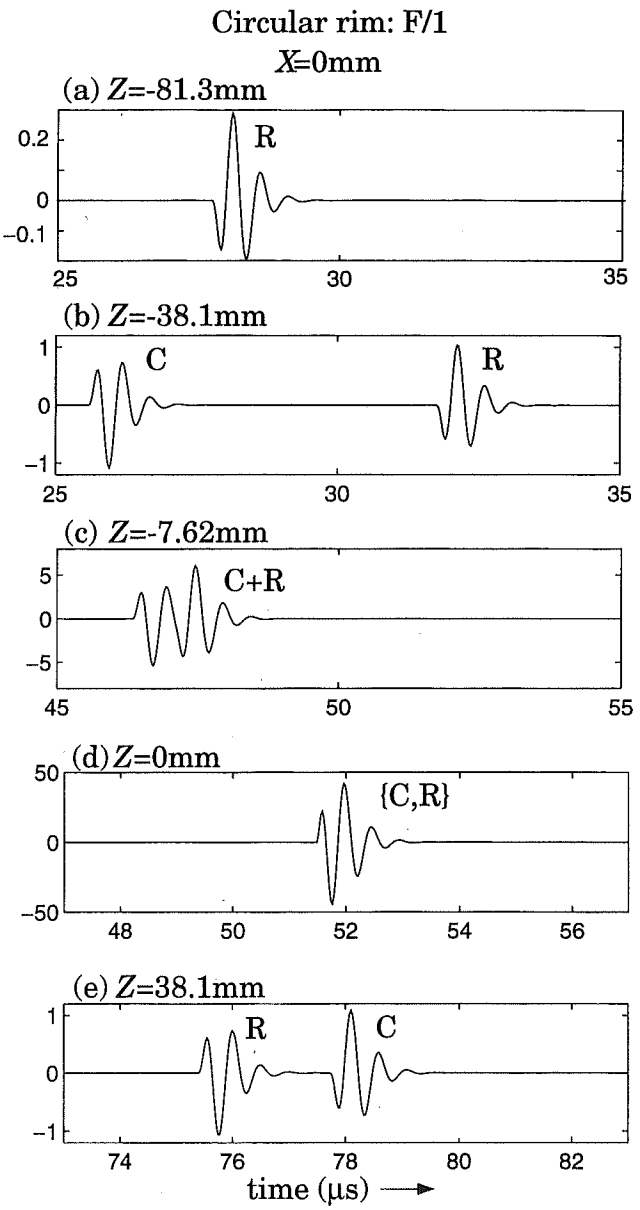

FIG. 6. Amplitude of radiated signal by $F/1$ transducer for observations along the aperture axis Z. Plots show signal strength and shape at various Z. Parameters as in Fig. 5. Letters C and R indicate part of the terms in Eq. (21) establishing the corresponding arrivals [see discussion after Eq. (24)]. C is associated with the travel time $(|\mathbf{x}|+a)/c_f$ and R with $(|\rho|)/c_f$. Both rim integration and on-axis closed-form expressions yield indistinguishable curves. Note that the signal strength behind the aperture ($Z=-81.3$ mm), due to rim diffraction, is relatively small but nonzero [see discussion following Eq. (50)].

$$\Omega_{\mathscr{A}}=\frac{1}{a}\int_{y_1=-b}^{b}\int_{y_2=-c}^{c}\frac{dy_1\,dy_2}{(a^2-y_1^2-y_2^2)^{1/2}}. \tag{69}$$

The expression at the right-hand side of Eq. (69) is evaluated by numerical integration.

VI. NUMERICAL RESULTS

In this section, numerical results are presented for a spherical-cap transducer and for a spherically curved

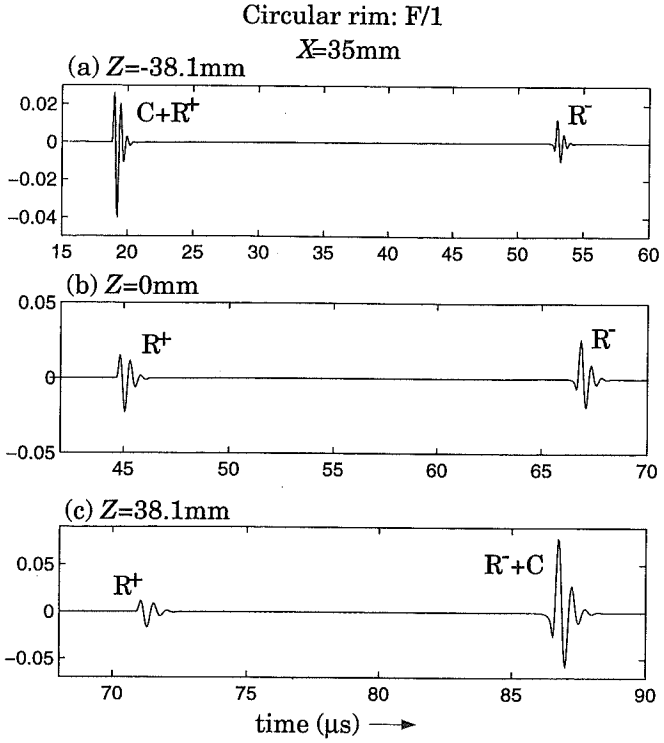

FIG. 7. Same as in Fig. 6, but for observation positions moved out from axis. Superscripts + and − indicate closest and farthest parts of the circular rim establishing the arrivals.

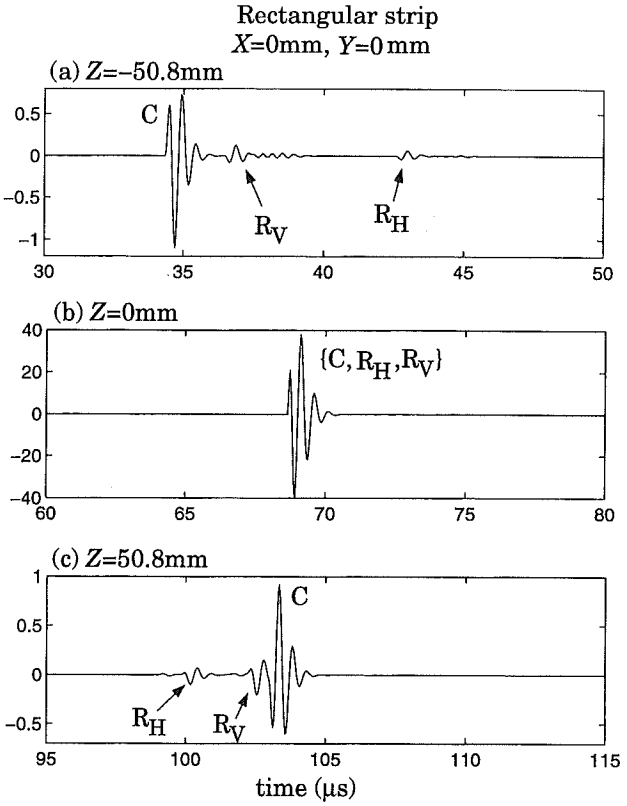

FIG. 8. Amplitude of radiated signal by the rectangular-strip spherical transducer for observations along the aperture axis Z. Plots show signal strength and shape at various Z. Parameters: $a=101.6$ mm, $b=50.8$ mm, $c=25.4$ mm (this rectangular transducer is equivalent to an $F/1$ along the vertical direction and to an $F/2$ along the horizontal direction). Letter C has the same convention as in Fig. 7. $R^{+,-}_{H,V}$ are shown in Fig. 3(b) and indicate parts of the rectangular rim establishing the corresponding arrivals; when both + and − parts have an equal arrival time, the superscript is omitted.

rectangular-strip transducer. In all cases the exciting acoustic pressure at the transducer's surface will be taken to be the causal, amplitude-modulated sinusoid

$$P_0(t)=A(t)\sin(\omega_0 t) \quad \text{for } \omega_0>0, \tag{70}$$

where the modulating amplitude function is given by

$$A(t)=\left(\frac{\alpha t}{\nu}\right)^{\nu}\exp(-\alpha t+\nu)H(t) \quad \text{for } \alpha>0, \quad \nu>0. \tag{71}$$

For $\nu=0$ the amplitude function has to be replaced by $\exp(-\alpha t)$. The oscillatory pulse has three adjustable parameters, of which ω_0 is determined by the center frequency $f_0=\omega_0/2\pi$, while α and ν are related to the rise time t_r and the width t_w of the modulating amplitude. The *pulse amplitude rise time* is defined as the value of t where $A(t)$ reaches its maximum value; it follows from Eq. (71) by putting the derivative equal to zero as

$$t_r=\nu/\alpha. \tag{72}$$

At $t=t_r$, we have $A(t_r)=1$. The *pulse amplitude time width* is defined as

$$t_w=\int_{t=0}^{\infty}A(t)dt. \tag{73}$$

Substituting Eq. (71) in Eq. (73) and carrying out the integration, we obtain

$$t_w=\frac{\Gamma(\nu+1)\exp(\nu)}{\nu^{\nu}\alpha}. \tag{74}$$

From Eqs. (72) and (74) it follows that

$$\frac{t_w}{t_r}=\frac{\Gamma(\nu+1)\exp(\nu)}{\nu^{\nu+1}}, \tag{75}$$

i.e., the parameter ν is determined by the ratio of the pulse amplitude time width and the pulse amplitude rise time. Figure 3 illustrates this relationship.

The time derivative of the pulse (which is needed for the evaluation of the wave field at the focus of the transducer) is found as

$$\partial_t P_0(t)=[\partial_t A(t)\sin(\omega_0 t)+\omega_0 A(t)\cos(\omega_0 t)]H(t). \tag{76}$$

Upon introducing the time-dependent phase angle $\psi=\psi(t)$ through

$$\partial_t A(t)=\{[\partial_t A(t)]^2+[\omega_0 A(t)]^2\}^{1/2}\sin[\psi(t)], \tag{77}$$

$$\omega_0 t=\{[\partial_t A(t)]^2+[\omega_0 A(t)]^2\}^{1/2}\cos[\psi(t)], \tag{78}$$

the right-hand side of Eq. (76) can be cast into the shape of an amplitude- and phase-modulated signal, viz.,

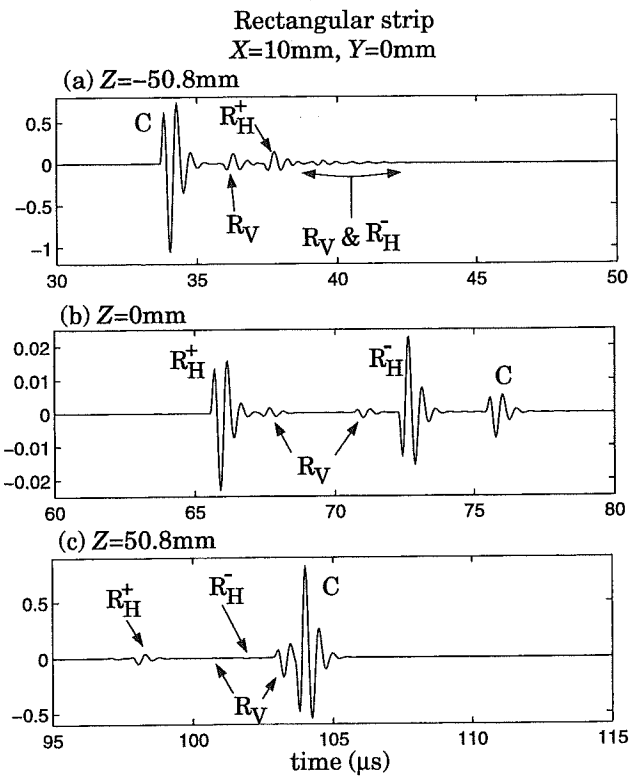

FIG. 9. Same as in Fig. 8, but for observation positions moved out from the axis along the vertical X direction.

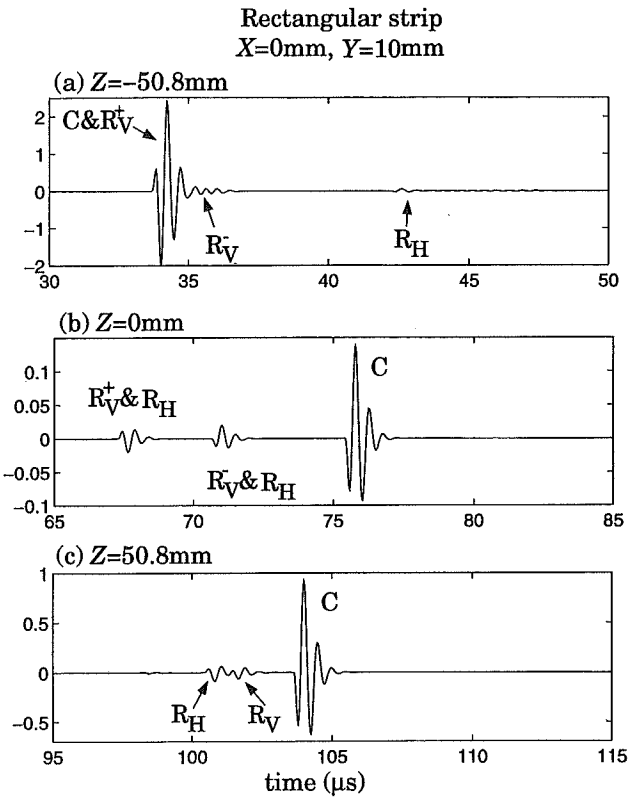

FIG. 10. Same as in Fig. 8, but for observation positions moved out from the axis along the horizontal Y direction.

$$\partial_t P_0(t)=\{[\partial_t A(t)]^2+[\omega_0 A(t)]^2\}^{1/2} \times\cos[\omega_0 t-\psi(t)]H(t). \tag{79}$$

To quantify the focusing power of the transducer, we introduce its *focal enhancement factor* $\Gamma_{\mathscr{F}}$ as the maximum value of the modulating amplitude in the right-hand side of Eq. (79). Differentiation with respect to t of the latter quantity shows that for the practical case where $\partial_t^2 A(t)+\omega_0^2 A(t)>0$, i.e., $\omega_0>\alpha/(\nu-1)^{1/2}$ and $\nu>1$ for our case, there is only a single maximum at $t=t_r$ whose value is ω_0. Using this value in the expression of Eq. (26) for the acoustic pressure at the focus, the focal enhancement factor is found as

$$\Gamma_{\mathscr{F}}=\frac{\Omega_{\mathscr{A}}}{4\pi}\frac{2\omega_0 a}{c_f}=\frac{\Omega_{\mathscr{A}}}{4\pi}\frac{4\pi f_0 a}{c_f}. \tag{80}$$

Note that this result holds for a focused transducer with an arbitrary rim.

The time Laplace transform of Eq. (70) is given by

$$\hat{P}_0(s)=(1/2j)[\hat{A}(s+\alpha-j\omega_0)-\hat{A}(s+\alpha+j\omega_0)], \tag{81}$$

in which Eq. (71) gives

$$\hat{A}(s)=\left(\frac{\alpha}{\nu}\right)^{\nu}\frac{\Gamma(\nu+1)}{s^{\nu+1}}\exp(\nu). \tag{82}$$

The spectral plot that shows $\log(|\hat{P}_0(j\omega)|$ as a function of $\log(|\omega|)$ for $\omega>0$ shows a slope of $-(\nu+2)$ as $|\omega|\to\infty$.

For our numerical results the values $f_0=2$ MHz, $\nu=2$, and $\alpha=5.71\times10^6$ s^{-1}, corresponding to $t_r=0.35$ μs and $t_w=0.65$ μs, have been selected. The corresponding pulse shape and its spectral amplitude are shown in Fig. 4(a) and (b), respectively.

A. The spherical-cap transducer

For arbitrary points of observation the right-hand side of Eq. (41) is evaluated by applying a trapezoidal integration rule, while the closed-form on-axis result of Eq. (50) has served as a check. With a uniform discretization of the rim integral into intervals of one and a half degrees, the two on-axis waveforms obtained were indistinguishable. For observation points close to the surface of the cone $\mathscr{K}$ that has $\partial\mathscr{A}$ as its directrix and $\mathscr{F}$ as its apex [see Fig. 1(b)], a more refined discretization is needed. The computation times involved were in the order of seconds on a workstation. Transducers of various degrees of focusing were considered. As an illustration, we present results for a highly focused one with an F number [$F/(a/d)$, following the conventional notation in ultrasonics[16]] of $F/1$. The transducer parameters are $a=d=76.2$ mm. Figure 5 shows an image of the events involved (superposition of a pulse with a travel time from the center of the transducer and a pulse with a travel time from the rim of the transducer), while Figs. 6 and 7 show actual waveforms at positions in various planes perpendicular to the axis of the transducer, viz., in a plane behind the center of the transducer [plot 6(a)], in planes in between the center of the transducer and its focal plane [plots 6(b), 6(c), and 7(a)], in the focal plane itself [plots 6(d) and 7(b)], and in planes beyond the focal plane [plots 6(e) and 7(c)]. Because the physics of transient radiation from circular rims has been reported exten-

sively elsewhere (see, for example, a good account in Ref. 4), we have reduced the description of these figures to the minimum included in the corresponding captions. The emphasis here is put on the versatility and computational efficiency of the solutions presented which allows for plotting and study of the transducer focusing properties and its dependence on the rim geometry. The focal enhancement factor for this transducer follows from Eq. (80) as $\Gamma_{\mathscr{F}}=86.7$. It should be noted, in particular, that unlike the present solution, the results based on the Rayleigh integral representation[1-4] do not yield the diffracted wave field behind the transducer.

B. The spherically curved rectangular-strip transducer

A transducer of this kind has also been analyzed by Ref. 6. We have taken the following dimensions: $a=101.6$ mm, $b=50.8$ mm, and $c=25.4$ mm. The rim integral is evaluated as indicated above. Numerical results are shown in Figs. 8–10 with the corresponding parameters and comments given in their captions.

VII. CONCLUSIONS

The transient acoustic wave field radiated by a focused transducer with a spherical radiating surface is evaluated by applying the Maggi–Rubinowicz transformation to the Kirchhoff–Huygens representation of the wave field. This transformation results in a line integral representation along the rim of the radiating aperture that holds for a rim of arbitrary shape, and for both planar and nonplanar radiators. The computation time needed to evaluate this (one-dimensional) integral is in the order of seconds on a standard workstation. For any shape of the rim, a simple time-domain expression for the acoustic pressure at the focus is also derived. Based on this expression we introduce a time-domain focal enhancement factor that characterizes the focusing properties of the transducer. The factor only contains the solid angle under which the transducer surface is viewed from the focus, the radius of the radiating spherical surface, the center frequency of the input signal, and the acoustic wave speed of the surrounding fluid. The expression holds for a general class of amplitude-modulated sinusoidal carrier waveforms of the initially launched acoustic pressure. For the transducer with a circular rim, a closed-form analytic expression is given for the on-axis acoustic wave field. This expression serves as a check on the accuracy of the numerical integration along the rim. Numerical results are presented for the transducer with a circular rim and for a spherically curved rectangular-strip transducer. Our analysis illustrates the versatility of the obtained rim integral representation. For example, this representation is ideally suited for modeling the action of a focused transducer as a source of acoustic radiation in more complicated geometries.

ACKNOWLEDGMENTS

The authors are thankful to A. K. Booer for support and for carefully reading the manuscript. We also thank one of the referees for valuable comments and suggestions.

[1] G. R. Harris, "Review of transient field theory for a baffled piston," J. Acoust. Soc. Am. **70**, 10–20 (1981).
[2] G. R. Harris, "Transient field of a baffled planar piston having an arbitrary vibration amplitude distribution," J. Acoust. Soc. Am. **70**, 185–204 (1981).
[3] P. R. Stepanishen, "Acoustic transients from planar axisymmetric vibrators using the impulse response approach," J. Acoust. Soc. Am. **70**, 1176–1182 (1981).
[4] H. Djelouah, J. C. Baboux, and M. Perdrix, "Theoretical and experimental study of the field radiated by ultrasonic focused transducers," Ultrasonics **29**, 188–200 (1991).
[5] F. Coulouvrat, "Continuous field radiated by a geometrically focused transducer: Numerical investigation and comparison with an approximate model," J. Acoust. Soc. Am. **94**, 1663–1675 (1993).
[6] P. Faure, D. Cathignol, and J. Y. Chapelon, "On the pressure field of a transducer in the form of a curved strip," J. Acoust. Soc. Am. **95**, 628–637 (1994).
[7] G. A. Maggi, "Sulla propagatione libera e perturbola delle onde laminose in un mezzo isotropo," Ann. Matematica (IIa) **16**, 21–48 (1888).
[8] A. Rubinowicz, "Eine einfache Ableitung des ausdrucks f'ur die Kirchhoffsche beugungswelle," Acta Phys. Polon. **12**, 225–229 (1953).
[9] A. Rubinowicz, *Die Beugungswelle in der Kirchhoffschen Theorie der Beugung* (Panstwowe Wydawnictwo Naukowe, Warszawa, 1957), pp. 97–103.
[10] A. Rubinowicz, "The Miyamoto–Wolf diffraction wave," in *Progress in Optics*, edited by E. Wolf (North-Holland, Amsterdam, 1965), Vol. 4, pp. 201–240.
[11] B. B. Baker and E. T. Copson, *The Mathematical Theory of Huygens' Principle* (Clarendon, Oxford, 1950), 2nd ed., pp. 74–84, 98, and 117.
[12] M. Born and E. Wolf, *Principles of Optics* (Pergamon, Oxford, 1987), 6th ed., pp. 449–453.
[13] C. J. Bouwkamp, "Diffraction theory," Rep. Prog. Phys. **17**, 35–100 (1954).
[14] A. T. de Hoop, "Time-domain reciprocity theorems for acoustic wavefields in fluids with relaxation," J. Acoust. Soc. Am. **84**, 1877–1882 (1988).
[15] A. T. de Hoop, "Reciprocity theorems for acoustic wavefields in fluid/solid configurations," J. Acoust. Soc. Am. **87**, 1932–1937 (1990).
[16] G. S. Kino, *Acoustic Waves: Devices, Imaging, and Analog Signal Processing* (Prentice-Hall, Englewood Cliffs, NJ, 1987), p. 185.